Rijksuniversiteit Groningen

BSc Thesis

Faculty of Mathematics and Natural Sciences

Experimental status and prospects in search for charged lepton flavor violation

Author:
Elianna Kraan

Supervisor:
Dr. Ir. C.J.G. Onderwater

April 15, 2016

Contents

1 Introduction

In Particle Physics, the Standard Model is the norm for all fundamental particles existing and the description of their interactions. One family of these particles are the leptons, consisting of three charged leptons (the electron, the muon and the tauon) and three neutrinos with corresponding flavors ν_e, ν_μ and ν_τ. This totals up to twelve leptons, since each lepton has its antiparticle. Neutrino oscillations are proof that lepton flavor is not conserved in the neutrino sector. Nevertheless, a flavor conservation law seems to hold for the charged leptons, meaning that a specific type of flavor cannot disappear in a leptonic decay.

This conservation law amongst many others relies on observations, as the Standard Model in its entirety is built upon experimental knowledge. However, even though it has been confirmed by many experimental observations, there is a lack of understanding as to why the Standard Model is built up the way it is currently believed to be. Therefore an experimental search for Physics Beyond The Standard Model, also called New Physics, continues to run at many of the worlds' largest physics research centers. Conservation of charged lepton flavor does not neccessarily hold in these new models and therefore lepton flavor violation might be found experimentally despite of the Standard Model. For a theoretical overview of the New Physics models concerning charged lepton flavor violation, see reference [1]. In this thesis we will focus on the experimental aspect of charged lepton flavor violation, by giving an overview of the experimental status and prospects on the search for charged lepton flavor violation (cLFV).

Some well-researched cLFV channels are rare muon decays ($\mu^+ \to e^+\gamma, \mu^+ \to e^+e^-e^+$), tau decays ($\tau^\pm \to \mu^\pm\gamma, \tau^\pm \to e^\pm\gamma, \tau \to 3\ell, \tau \to \ell + h(s)$), rare kaon decays ($K_L^0 \to e\mu, K^+ \to \pi^0 e^\pm \mu^\pm$), lepton conversions ($\mu^- A \to e^- A, \mu \to \tau$) and processes involving hadronic resonances* or heavy quarks [2].

According to the Standard Model, the chance of observing such a lepton flavor violating decay is practically zero. But when looking for New Physics, some rare decays might be observable. Until now, no such charged lepton flavor violating decay has been observed, but the limit on the branching ratios (also branching fractions, symbol: B), the ratio in which we express the results, is getting more stringent after each new result.

*a hadronic resonance is an excited state of a hadron

The branching ratio is the fraction of particles decaying in one specific mode, in our case a lepton flavor violating mode, divided by all the possible decay modes. These other decay modes are generally referred to as background events. Typical theoretical branching fractions for cLFV processes according to the Standard Model are of the order $O \sim 10^{-44}$ or even smaller. In the searches for cLFV, the aim is to set a smaller upper limit onto this ratio than the previous one, or to ultimately obtain a positive result. It should be noted however that in case of a Standard Model branching fraction, it is safe to assume that the latter will never be possible. This upper limit on the branching ratio as the final experimental result is usually referred to as the sensitivity of the experiment.

The branching fraction cannot be measured better than 1 divided by the number of particles produced, which would be in the case of zero background. In general the background for a cLFV experiment is much larger than the signal event, so that the uncertainty of the signal event can never be smaller than the uncertainty in the background signal.

To analyze the experiments on cLFV, it is interesting to look at the two main compounds of precision experiments: systematics and statistics, including the respective systematic and statistical errors. The systematics of an experiment comprises of how easy it is to recognize the lepton flavor violating decay out of the background events, whereas the statistics of an experiment mainly depends on how many particles (muons, taus, kaons etc.) are created per year and which part of those particles consists of background.

In this thesis, we investigate the essential factors in several cLFV experiments, where most attention is paid to muon experiments, since they are the most precise. In chapter 2, we present the most recent experiments and future projects looking for muon decays, in chapter 3 we describe the current and future status of tauon decays, meson decays and other relevant cLFV experiments and finally in chapter 4 we come to a conclusion.

2 Muon decays

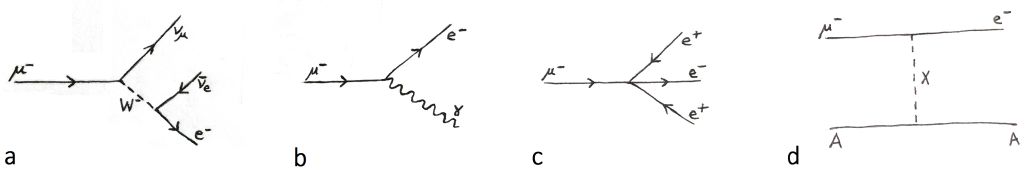

Figure 1: (a) muon Michel decay (b) $\mu^+ \to e^+\gamma$ (c) $\mu^+ \to e^+e^-e^+$ (d) muon conversion, where A is a nucleus and X an undefined particle*

According to the Standard Model, a muon decays into an electron, an electronneutrino and a muonneutrino, as proposed by Pauli in 1930 [3]. The distribution of the momenta of the outgoing particles is given by the so-called Michel distribution. Hence this decay is often referred to as muon Michel decay. Of the rare lepton flavor violating decays are just a few channels possible because of energy-momentum conservation, of which the most important ones are $\mu \to e\gamma, \mu \to eee$ and muon conversion, see Feynman diagrams in Figure 1.
A muon will live for about 2.2 μs, which makes it relatively easy to detect [4].
The first experiment ever which was intended to look for cLFV was done in the late 1940s by Hincks and Pontecorvo [5]. The unobserved $\mu \to e\gamma$ had a great impact on the development of particle physics, since it made the existence of the muon as an independent particle from the electron clear. From this it also followed that there is a muonneutrino next to the already discovered electronneutrino.

2.0.1 Muon beams

Experiments looking for $\mu \to e\gamma$ and $\mu \to eee$ are only performed with positive muons because negative muons are captured by an atom as a heavier form of an electron, whereas this problem does not arise for positive muons, making an experiment better controllable. As for muon conversion, the previous does not hold and negative muons are used, since the idea is that a muon is captured by a nucleus.

*its nature is dependent on which New Physics model is chosen

Intense muon beams can be obtained by either hitting light targets with low-energy protons or from by-products of high-energy collisions at proton accelerators [2]. From proton irradiation on a target pions are created and from charged pion decays muons can be obtained.

For the statistical strength of an experiment a high-rate muon beam is needed, whereas for the systematical strength of an experiment a minimized beam-related background is required, meaning that as much as possible pions should be filtered out. In experiments searching for $\mu^+ \to e^+\gamma$ and $\mu^+ \to e^+e^-e^+$ decays a continuous muon beam is used whereas the experiments looking for muon conversion make use of a pulsed muon beam. The reason for this difference are the different dominant background sources.

For $\mu \to e\gamma$ decay, the dominant background comes from the accidental background of a positron from muon Michel decay coinciding with a photon coming from another muon decay (for details, see Section 2.1). This means that two different muon decays are required for one background event, so that the rate of accidental coincidence events is proportional to the μ^+ rate squared, whereas the rate of the signal events is directly proportional to the μ^+ rate. Then the signal to noise ratio, indicating the amount of signal events as a fraction of the accidental coincidence background events, is inversely proportional to the μ^+ rate. Thus for an equal total amount of muons and an equal time interval for both types of beams, using a continuous muon beam results in a better signal to noise ratio than for a pulsed beam.

For $\mu^+ \to e^+e^-e^+$ decay, similar arguments as for the $\mu^+ \to e^+\gamma$ decay hold as to why a continuous muon beam is used, even though the accidental background is not the dominant one (see Section 2.2). The effect on the signal to noise ratio is even stronger since the 3-body decay signature requires the rate of accidental coincence events to be proportional to the μ^+ rate to the third power.

For muon conversion, the dominant background is beam-correlated, coming from beam impurities which are mostly pions [6]. Due to the short lifetime of muons it is possible to use a pulsed muon beam and then detect electrons in the time interval between the pulses to minimize the beam-correlated background.

In the left half of Figure 2 a typical muon-beam production setup can be seen. To reduce beam-related background, the proton beam is counterdirected with respect to the resulting muon beam. In this way pions cannot reach the

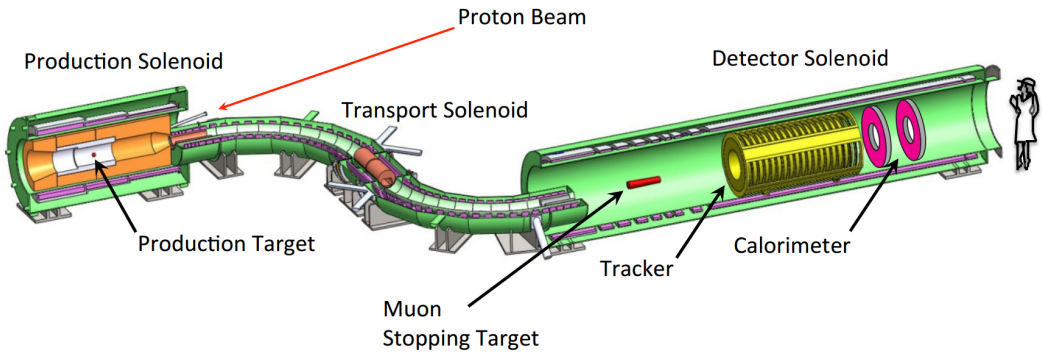

Figure 2: Schematic layout of the Mu2e muon conversion experiment. From [7].

experiment and only muons from the stopped pions will reach the interaction region, in particular those at the surface of the target which is why they are called surface muons and also why the beam is called a surface muon beam. These surface muons are favorable to work with because of a relative high production rate, a high enough velocity to transport them from the proton source* to the experiment and a relative low energy which makes them easier to stop. For all three types of muon decays that will be discussed here the surface muons have to be stopped, since for stopped muons the momentum and energy of the initial state are well defined. This will help to enhance the sensitivity of these experiments, as will be shown later.

*Due to high radioactivity caused by the proton beam, the experiment has to be physically separated from the proton source.

2.1 $\mu^+ \to e^+\gamma$

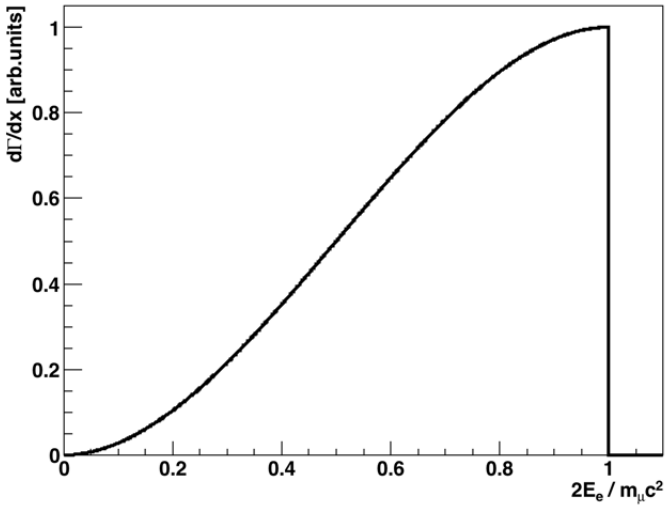

Figure 3: Michel decay energy spectrum

For the Standard-Model favored $\mu^+ \to e^+\bar{\nu}_\mu\nu_e$ decay, the muon energy is divided over three particles so that the energy spectrum of the positron is continuous, as pictured in Figure 3. The endpoint of the spectrum is given by the highest possible electron energy, which is equal to half the muon rest mass $\frac{1}{2}m_\mu c^2$. This corresponds to an energy of ∼52.8 MeV [8].

When a muon decays into a positron and a photon, the positron and the photon will be created back to back to cancel out each others momentum because the incident muon has been stopped and has therefore no momentum. This decay is found typically by looking at the energy spectrum of the positrons: the positron mass is negligible, making a mono-energetic positron and photon with both half the energy of the muon mass. The mono-energetic positrons would be visible as a peak in Figure 3, theoretically a delta function but due to finite experimental resolution somewhat widened, positioned exactly at the endpoint of the Michel spectrum. One of the important experimental requirements is therefore an energy resolution high enough to separate the signal from background events.

The positron with the typical energy has to be measured simultaneously with

a photon of energy $E_\gamma = p_\gamma = p$ to find $\mu \to e\gamma$. However, there are two types of background resulting in the same signal that should be considered [9]:

- the radiative muon decay (RMD), which is the physical background where the positron coming from usual muon Michel decay interacts with matter in which a photon is created ($\mu^+ \to e^+\gamma\bar{\nu}_\mu\nu_e$) and
- the accidental background, where the positron from muon Michel decay coincides with a photon coming from RMD, positron-electron annihilation-in-flight ($e^+e^- \to \gamma\gamma$) or bremsstrahlung ($e^+A \to e^+A\gamma$).

2.1.1 The MEG experiment

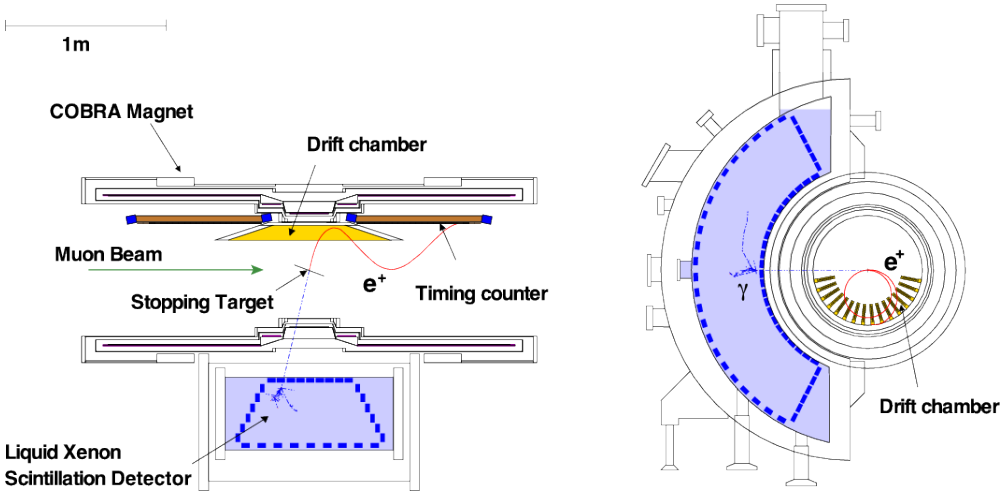

Figure 4: Schematic layout of the MEG experiment, top view on the left and side view on the right. From the target one simulated event is shown. From [10].

The most recent result on $\mu \to e\gamma$ was found at the MEG (Muon to Electron and Gamma) experiment [10], located at the Paul Scherrer Institute (PSI) in Switzerland and published in 2013 [9,11]. The current best upper limit on the branching ratio is 5.7×10^{-13} (90% confidence level), which is four times more stringent than the previous best limit set by MEG.
The following description relies heavily on reference [10] and some values were taken from reference [6].

The experimental setup can be seen in Figure 4. Positive muons are stopped at a target in the middle of a magnetic spectrometer to measure the electron intensity spectrum as a function of energy. Here the muons would decay in a positron-photon pair. Each event is described by a set of five observables: the positron and photon energy, their relative angles in the horizontal and vertical plane and the relative emission time [9]. The positron track is measured by a set of Drift CHambers (DCH) and the positron time by a Timing Counter (TC) which consists of scintillation bars read out by photomultiplier tubes.

The muon beam is one of the world's highest intensity continuous muon beams and its rate is higher than 10^8 μ^+/s with an optimal suppression of beam-correlated background. The muon stopping rate in the target which is apart from the beam intensity also dependent on the detector performance and its sensitivity to the $\mu^+ \to e^+\gamma$ decay is optimalized for 3×10^7 detectable decays per second.

A superconducting magnet, COBRA (COnstant Bending RAdius), creates a magnetic field that is used to measure the positron momentum from its radius of curvature in the field. The field is shaped such that the bending radius of the positrons is only weakly dependent on their emission angle while also filtering out the low-momentum Michel positrons. Positrons emitted perpedicular to the incoming muon beam are deflected so that they do not turn repeatedly into the drift chambers. To fulfill these requirements the magnet generates a magnetic field of which the strength gradually decreases at increasing distance along the magnet axis (z-axis) from the center. The MEG experiment is the first among particle physics experiments to make use of a gradient magnetic field. Comparing the effect of COBRA on the perpedicularly emitted positrons to a uniform solenoidal field, the positrons would turn repeatedly in the spectrometer instead of being deflected from it.

The DCH system consists of 16 modules aligned in a half circle inside the bore of COBRA. To reduce multiple Coulomb scattering, which limits the momentum resolution, and to minimize the accidental γ-ray background by positron annihilation-in-flight, the modules are filled with a low-mass helium-based gas mixture. The DCH modules also have as low-mass construction so that the average amount of material along the positron track sums up to only $2.0 \times 10^{-3} X_0$*. The resolution with which the radial coordinate can be

*The radiation length X_0 equals the mean distance over which a positron loses all but $\frac{1}{e}$ of its energy

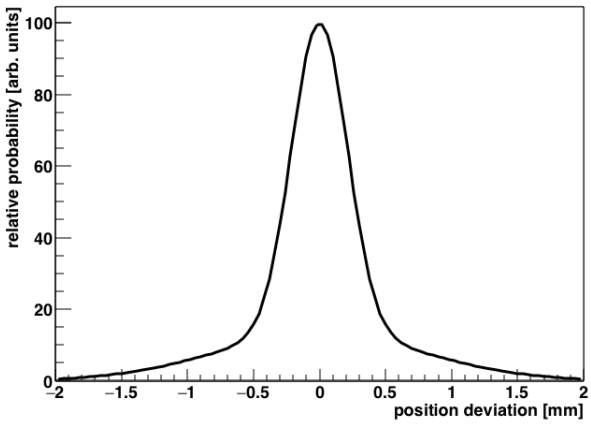

Figure 5: DHC radial coordiate resolution described by a combination of two Gaussians, with a main resolution of 210 μm (87%) and a remaining resolution of 780 μm (13%).

detected can be estimated by a combination of two Gaussians which results in a main resolution of 210 μm (87%) and a resolution of 780 μm for the remaining 13%. This combined radial resolution is illustrated in Figure 5. For the z coordinate resolution the same approximation holds resulting in a main resolution of 800 μm (91%) and a resolution of 2.1 mm for the remaining 9%. The average energy resolution, also best fitted by a double Gaussian, is 306 keV for the main part (82%). Since the $\mu^+ \to e^+\gamma$ branching ratio can be estimated as the cLFV signal as a fraction of the Michel signal*, where both the cLFV signal and the Michel signal have their own *absolute* efficiency, only the *relative* efficiency of signal positrons with respect to Michel positrons is relevant in the analysis. This relative efficiency is $\sim$70%.

The positron emission time at the muon target is measured by the Timing Counter with a total accuracy of $\sim$107 ps by correcting for the track length obtained from the DCH system. Whereas the actual and design resolution are about equal, the actual efficiency of about 50% is far below the design efficiency of >90%. This is apparently of no consequence, as no elaborate discussion on this low efficiency was found in the literature.

The photons are detected by a C-shaped scintillator filled with 900 liters of

*The denominator of the branching fraction contains all possible muon decays, but the effect of the non muon Michel decays is negligible for the final ratio.

Liquid Xenon (LXe) and with 846 photomultiplier tubes submersed in the liquid. To minimize the dominant background of accidental coincidences, a high light yield is required to achieve excellent energy, time and position resolutions while the fast LXe decay time is beneficial for reducing pile-up events. The average energy resolution of the LXe detector varies from 1.7% (main part) to 2.4% (close to the inner surface)*, and the average timing resolution, z coordinate resolution, angular resolution and radial resolution are respectively 67 ps, 5 mm, 5 mm and 6 mm [6]. The detector efficiency is 63%. The effective volume of the LXe detector (the dashed blue outlined area in Figure 4) determines the angular acceptance of the experiment, which results in a total acceptance of ∼11%.

The global timing resolution for a $e-\gamma$ coincidence has been estimated from RMD observation and is found to be 122 ps.

2.1.2 The MEG II experiment

Resolutions	MEG	MEG-II
e^+ energy (keV)	306 (main)	130
$e^+\theta$ (mrad)	9.4	5.3
$e^+\phi$ (mrad)	8.7	3.7
e^+ vertex (mm) Z/Y(main)	2.4/1.2	1.6/0.7
γ energy (%) (<2 cm/>2cm from inner surface)	2.4/1.7	1.1/1.0
γ position (mm) (z/angular/radial)	5/5/6	2.6/2.2/5
$\gamma - e^+$ timing (ps)	122	84
Efficiency (%)		
γ	63	69
e^+	40	88

Table 1: Expected resolutions and efficiencies for the upgraded experiment compared to the present values, taken from ref. [6]

The following paragraph closely follows the descriptions given in reference [6] and [9].

An upgrade proposal for the MEG experiment which will be called MEG II has been approved in 2013. Table 1 charactarizes the improvements planned

*Due to a discrepancy between the photon energy resolutions given in ref. [6] and [10], the values given here correspond to the latter, which is the most recent of the two.

upon the upgraded experiment. In this table a selection of critical aspects in detection efficiency, as discussed in the previous section, can be recognized in some form. Positron angular resolution is described by θ (horizontal plane) and ϕ (vertical plane) and the vertex, which indicates the position of muon decay in the target, is described by two spatial resolutions Y and Z. Both positron energy and vertex resolution are described by a double Gaussian, which is why the main resolution is indicated. It can be seen that the resolutions are typically improved by a factor $\sim$2, leading to a highly improved detector sensitivity. In the following section, a more in-depth discussion on part of the improvements is given.

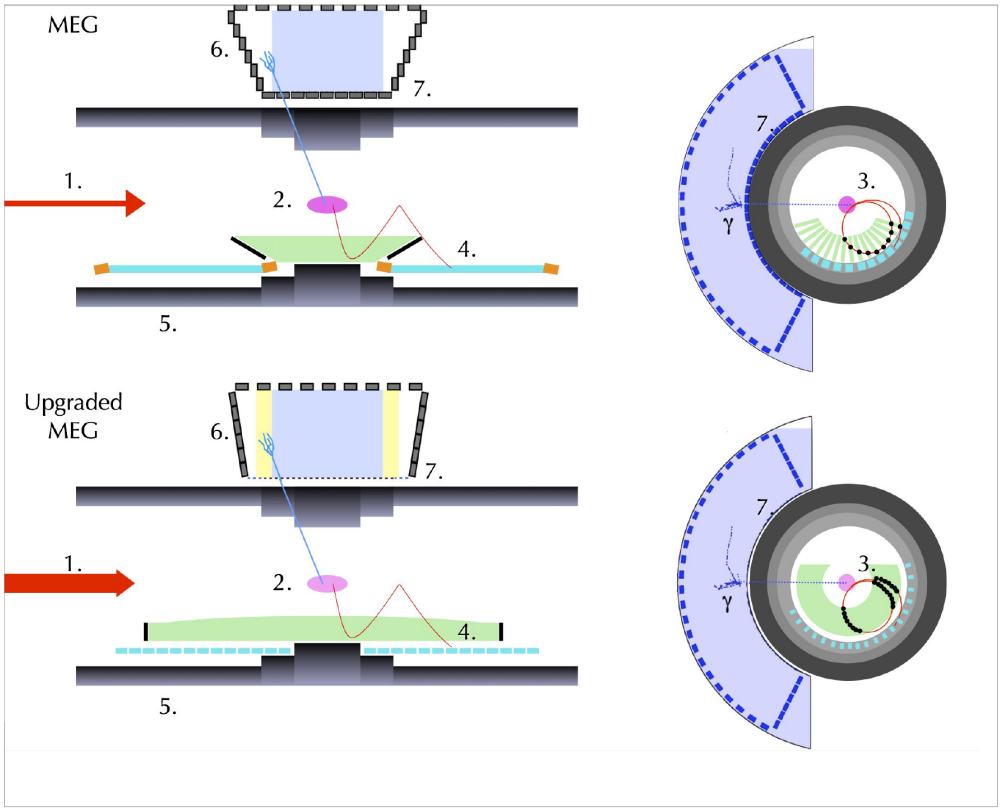

Figure 6: The MEG II experiment (above) compared to the MEG experiment (below). The numbers correspond to the items listed in the text. From [6].

There are seven key changes in the new detector setup and one key improvement related to the recording and processing of the detector signals that will not be discussed any further. In Figure 6 each of the seven improvements is indicated on the schematic layout of the detector systems.

1. A higher muon beam intensity will increase the muon stopping rate to at least 7 $\times 10^8$ μ^+/s . The increased rate has to be parallel to an increased detector efficiency and improved experimental resolutions to compensate for the increase in background events.

2. The target thickness will be reduced to minimize multiple scattering on the positron and photon trajectories.

3. The DCH system will be replaced by a new single volume drift chamber to obtain a reduced radiation length and improved resolutions and efficiency.

4. The new positron tracker is extended to measure the positron trajectory to the Timing Counter to improve the positron timing resolution and the positron reconstruction efficiency.

5. The Timing Counter will be replaced by a highly segmented one with an improved estimated timing resolution of 35 ps.

6. The LXe detector will have an extended acceptance in the z-direction of 10% on each side, indicated in yellow in Figure 6, to reduce energy leakage at the side surfaces leading to better energy resolutions.

7. The LXe detecter energy, position and timing resolutions will be increased for photon events close to the inner surface.

Due to the enhanced precision of each component of the setup a much better separation of signal from background events can be realized. The reduced accidental background allows for a higher muon stopping rate in the new detector. Optimization studies on different beam intensities possibly containing lower-momentum muons and on various corresponding target types and thicknesses have been performed. The combined effect of the new positron detector together with less positron scattering from the thinner target will lead to better spatial and energy resolutions for the positron detection.

The LXe detectors' energy and spatial resolutions in the previous setup are limited by the non-uniformity of the PMT coverage on the surfaces and the PMT size, especially for shallow events. Therefore the current PMTs on the inner surface will be replaced by a larger number of smaller photosensors to improve these resolutions. The PMTs on the side surfaces will be placed in a different configuration to optimize resolutions for photon events close to the side surfaces.

The MEG II experiment is expected to run for three years starting from 2016. A branching fraction of 6×10^{-14} is aimed for, which is one order of magnitude smaller than the current upper limit.

2.2 $\mu^+ \to e^+e^-e^+$

As the back to back signature emission for $\mu \to e\gamma$ decay, the kinematical signature for $\mu^+ \to e^+e^-e^+$ decay is that of a 3-body decay, meaning that all three electrons* are emitted in the same plane with zero total momentum. The sum of their energies totals up to the muon mass minus three electron masses, setting an invariant mass constraint for signal events. Additionally, each electron can have at most half of the muon mass due to phase space constraints. Detection techniques also differ from $\mu \to e\gamma$ decay, since only charged particles and no photons have to be detected.

Again, the background consists of a physical and an accidental one due to finite resolutions in an experiment, however the physical background is now the dominant one. The main irreducible physical background is the internal conversion decay $\mu^+ \to e^+e^-e^+\bar{\nu}_\mu\nu_e$, equivalent to RMD ($\mu \to e\gamma\bar{\nu}\nu$) where the photon converts into an e^+-e^- pair during the decay. Both the zero momentum and the invariant mass constraint do not hold for internal conversion. Since the amount of energy converted into neutrinos is negligible, only the momentum carried away by the neutrinos makes this background distinguishable from signal events. Therefore a very good momentum resolution is needed for suppressing the internal conversion background [12].

The accidental background comes from two muon Michel decay positrons coinciding with an electron coming from another source such as photon conversion, Bhabha scattering† or a wrongly reconstructed positron. Apart from not fulfilling the kinematical constraints, these accidental events have no common vertex and are not coincident, so excellent position, timing and momentum resolutions are required to reduce this background [12].

*electrons refer to both electrons and positrons in the $\mu^+ \to e^+e^-e^+$ section

†an incoming electron and positron scatter into an outgoing electron-positron pair

2.2.1 The SINDRUM experiment

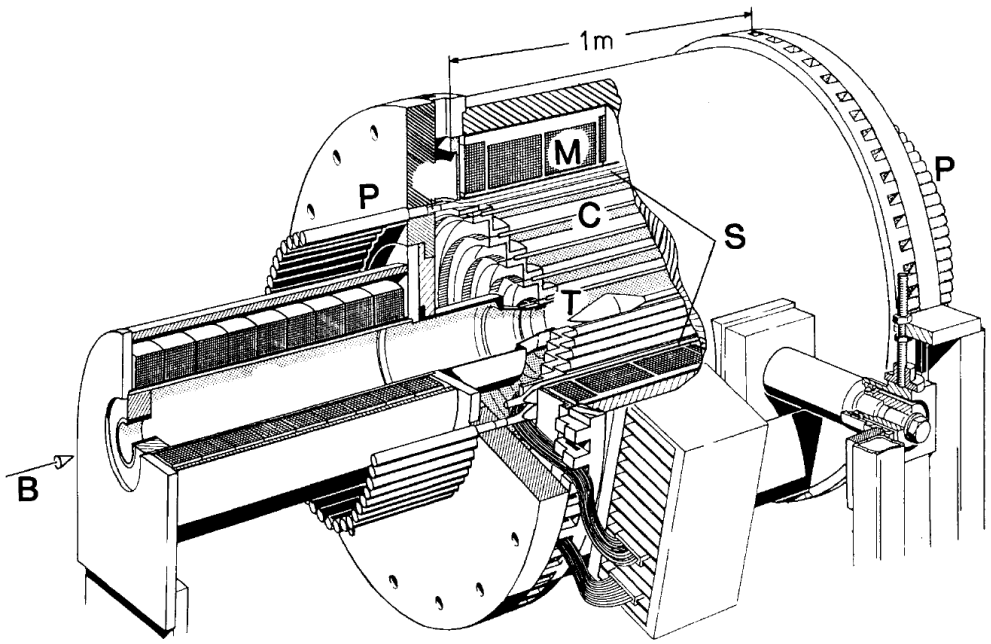

Figure 7: A schematic view of the SINDRUM spectrometer. B: muon beam, T: target, C: multiwire proportional chambers, S: scintillators, P: PMTs, M: magnet coil. Adapted from [13].

The current best upper limit of 1.0×10^{-12} on the $\mu \to eee$ branching fraction was set in 1986 at the former Swiss Institute for Nuclear Research (SIN is now a part of PSI) with the SINDRUM magnetic spectrometer, which was operating since 1983 [14]. The experimental description given in Reference [13] will be followed closely here, although some statements were taken from reference [14] and [15].

The experimental setup can be seen in Figure 7. The positive muons are stopped in a hollow double-cone shaped target located at the middle of the cylindrical spectrometer with a muon stopping rate of $\sim 5 \times 10^6$ [14]. The target is surrounded by five low-mass concentric multiwire proportional chambers (MWPCs) to measure the charged particle tracks with a radiation length of $0.08X_0$ to $0.17X_0$ per layer. The relative momentum resolution is 5.1/3.6% for particles with a momentum of 50/20 MeV/c and the angular

resolution is 28 mrad for 20 MeV/c particles. The vertex resolution is about 1 mm. The MWPCs are surrounded by a cylindrical array of scintillator strips for timing signals with a resolution of less than 1 ns. Finally the scintillators are surrounded by the magnet coils producing a homogeneous field parallel to the main cylindrical spectrometer axis (z-axis). The acceptance, given as the probability for all three particles to reach the scintillators, is 0.24 for signal events and 2.1×10^{-4} for internal conversion events. The combined achieved timing and momentum resolutions were sufficient to suppress the accidental background completely.

The gas filled MWCPs and plastic scintillator strips are similar to the MEG DCH system and Timing Counter, respectively. The main differences are the absence of a photon detector, the double-cone shape of the target as opposed to the elliptically shaped MEG target and the homogenety of the magnetic field as opposed to the gradient field of the MEG spectrometer.

2.2.2 The Mu3e experiment

At PSI a new project Mu3e which will look for the $\mu^+ \to e^+e^-e^+$ decay is currenly under development. The experiment will be performed in two phases, an exploratory first phase planned to start in 2016 and a second phase with a new high-intensity beamline starting after 2017 [12, 15].
This section relies strongly on reference [15], unless stated otherwise.

The exploratory phase, which is split up in two subphases IA and IB, will make use of the same muon source as MEG. Besides commissioning and validating the experimental techniques, the aim is to push the existing upper limit by three orders of magnitude, meaning a limit on the branching fraction of 10^{-15}. During this stage only part of the final setup is used. The final goal is to exclude a branching fraction larger than 10^{-16} at 90% confidence level during phase II, for which a High-intensity Muon Beam (HiMB) with a rate above 2×10^9 μ^+/s will be needed.

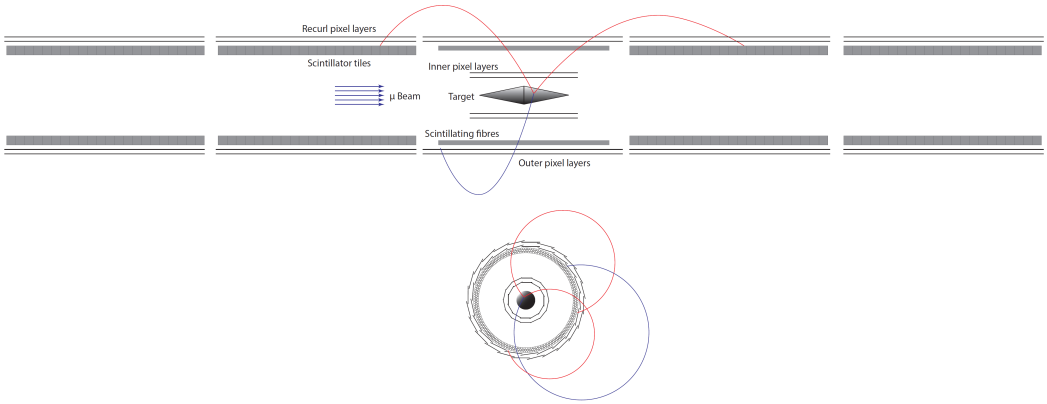

Figure 8: Schematic layout of the final phase Mu3e detector, top view above and side view below. Adapted from [15].

In figure 8 the final phase experimental setup divided in five independent stations is shown including a simulated event. The red lines represent positron tracks and the blue line an electron track. In phase IA the setup will only consist of the central station containing the target, but without the scintillating fibres. In phase Ib two recurl stations will be added on each side of the central station which now includes scintillating fibres. The final setup in phase IB consists of five stations; the central station and two recurl stations on each side.

The setup is built inside a solenoid magnet producing a homogeneous field needed for guiding the muon beam to the target and precise electron momentum measurements. In phase I, the present muon beam at PSI is expected to deliver its highest possible rate of $\sim 1 \times 10^8$ μ^+/s, which will then be the only limiting factor in the sensitivity. The second phase muon source HiMB, which is based on the production of surface muons just as the present source, is currently under study. To achieve the ultimate sensitivity aimed for, it needs to provide an unpulsed muon stopping rate of the order 10^9 detectable muons per second.

The target is designed to contain enough material in the beam direction to stop most of the surface muons while at the same time having a minimal thickness in the electron decay flight direction to reduce multiple scattering and thus reduce loss in momentum resolution. The target should also have a large surface to be better able to separate tracks coming from diffferent muon decays so that the accidental background events are reduced.

Electron momenta are measured by layers of ultra thin silicon pixel tracker with a timing resolution of 20 ns and a radiation length of $\leq 0.001 X_0$ to reduce Coulomb scattering, which is the dominating factor affecting the momentum resolution. For the same reason the detector layout is designed specifically to measure recurling tracks, since after exactly half a turn the effects of multiple scattering cancel in first order with respect to the electron track deflection. With the recurl stations the passing of the electron track can be detected multiple times.

Two scintillator timing systems improve the capability for event building and suppression of accidental background. Four radial pixel layers in the central station allow for precise momentum and vertex measurements and are supplemented by a scintillating fibre tracker for precise timing measurements in phase IB and phase II. The fibre tracker with a resolution of several 100 ps and an efficiency close to 100% is only needed in the advancing phases to resolve accidental background events at higher muon decay rates. At the same time it serves to determine the charge of electron tracks by measuring their direction of propagation as a function of time in order to identify an electron track either as a new event or as a recurling track of an already measured electron.

Each recurl station consist of two pixel layers around one layer of scintillating tiles with a timing resolution of less than 100 ps and a much larger thickness than the fibre tracker since the electrons are stopped here. The recurl stations significantly add precision to the momentum measurements and will thereby contribute to the suppression of internal conversion background. Another advantage is the possibility to sustain higher rates, since tracks are further apart in the recurl stations.

2.3 $\mu^- A \rightarrow e^- A$

This section and the following sections strongly rely on references [8], [16] and [17], unless indicated otherwise.

Another possible muonic cLFV channel is the process of a negative muon being trapped by an atomic nucleus after which the muon converts into an electron, known as muon conversion. Additionally, the muon can undergo two other possible non flavor violating processes, namely muon decay in orbit (μ-DIO: $\mu^-(A,Z) \rightarrow e^- \nu_\mu \bar{\nu}_e (A,Z)^*$) and muon capture ($\mu^-(A,Z) \rightarrow e^- \nu_\mu (A, Z-1)$).

The kinematical signature for coherent muon conversion, the dominant conversion process where the nucleus ends up in the ground state, is a monoenergetic electron with an energy of $E_{\mu e} \sim m_\mu - B_\mu$, where m_μ is the muon mass and B_μ is the binding energy of the muonic atom. This energy is therefore dependent on the chosen target material nuclei intended to form the muonic atoms, which may differ depending on the experiment. These typical electron energies, for example 104.3 MeV for titanium and 94.9 MeV for lead, are experimentally favorable because they are far above the ~52.8 MeV endpoint energy of the muon Michel spectrum. Another favorable aspect of muon conversion experiments is the single electron event signature, as opposed to the multiple particle signal events of the two precedingly described muonic cLFV searches. Because of this single signal no coincidence measurements are required and thus a high intensity muon beam can be used without the negative consequences of an accidental background.

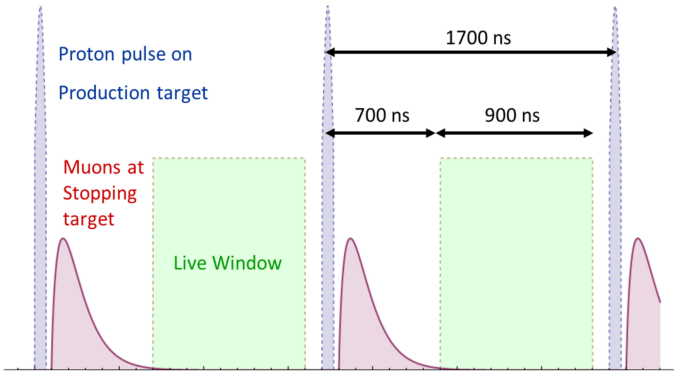

Figure 9: Mu2e pulse structure and live window. Adapted from [7].

*A: mass number, Z: atomic number or proton number

There are three main background sources of electrons with an energy around 100 MeV*:

- The intrinsic physical background, of which the relevant one is muon decay in orbit, as mentioned above. This background peaks at an energy below the kinematical endpoint of free muon decay, but has a steeply falling high-energy tail overlapping with $E_{\mu e}$.
- The prompt beam-related background mainly consisting of radiative pion capture (RPC: either $\pi^- A \to \gamma A'$ followed by photon decay into an e^+-e^- pair or internal conversion given by $\pi^- A \to e^+ e^- A'$) and pion (π-DIF) and muon (μ-DIF) decay in flight
- Cosmic ray (induced) electrons and reconstruction errors

As seen before in the other muon experiments, the experimental design for a muon conversion search will be based on suppressing these backgrounds.

High-Z materials are preferred for the muon stopping target, as the muon conversion rate increases and the endpoint of the μ-DIO spectrum decreases inside a higher-Z material.

Unlike the muon beams of experiments looking for $\mu \to e\gamma$ and $\mu \to eee$, negative muons are obtained from pulsed beams for muon conversion experiments to suppress beam-related background, as explained in Section 2.0.1. An illustration of this principle can be seen in Figure 9, where the pulse structure and the live window, the interval in which the measurements are taken, of the Mu2e experiment (Section 2.3.3) are pictured.

There are currently no running experiments in search for muon conversion, however two large-scale (Mu2e and COMET) and one small-scale (DeeMe) muon conversion experiments are in development.

Mu2e and COMET are based on the MECO experiment, which was developed at Brookhaven National Laboratory (BNL) in the United states but was cancelled in 2005 due to funding issues. Its key principles for background suppression are inspired by the MELC proposal at the Moscow Meson Factory. Many similarities thus hold between Mu2e and COMET with regard to these key elements which are related to beam pulsing, a magnetic pion capture system and curved muon transport solenoids, as will be discussed in Sections 2.3.3 and 2.3.4.

*Note that on pages 51 (bottom) and 52 (top) of reference [17] electrons generated by neutron-generated photons are noted as the most common background.

2.3.1 The SINDRUM II experiment

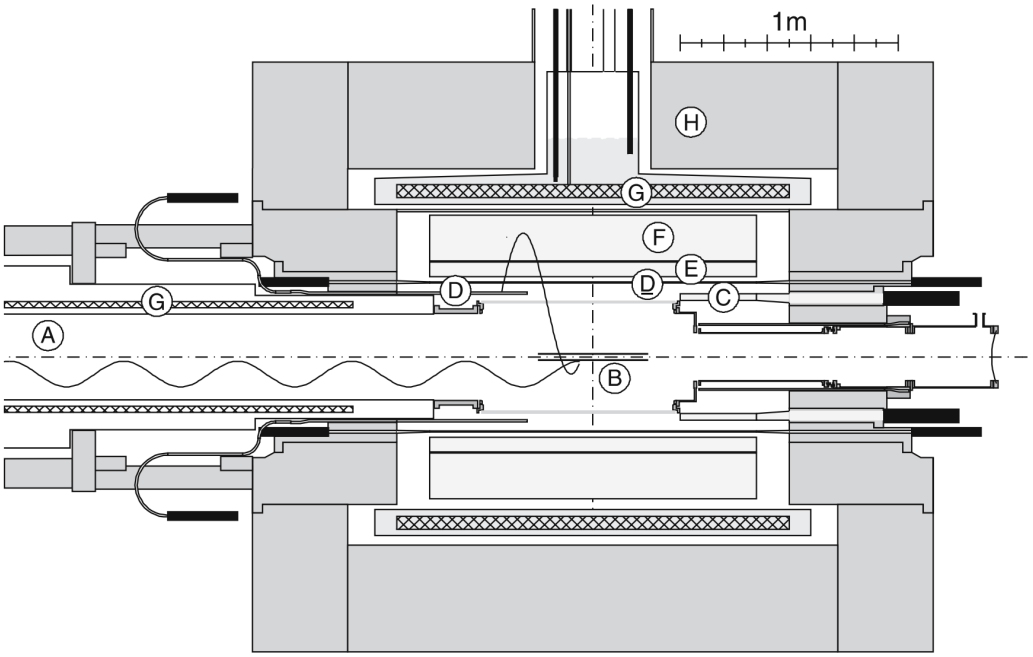

Figure 10: The SINDRUM II spectrometer, configuration as in 2000. A: exit beam solenoid, B: gold target, C: Cherenkov detector, D: scintillator detector, E: inner drift chamber, F: outer drift chamber, G: superconducting coil, H: magnet return yoke. Adapted from [18].

The most recent project to search for muon to electron conversion has been executed with the SINDRUM II spectrometer at PSI. The search resulted in upper limits on the branching fractions of $\mu - e$ conversion in muonic gold, titanium and lead, as summarized in Table 2.
The experimental description given in this section is strongly based on reference [18].

In figure 10, a schematic layout of the cylindrical SINDRUM II spectrometer can be seen. Along the solenoid axis the typical spiraling path of an incoming muon is indicated and originating from the gold target (B) a simulated electron event is shown, which also follows a helical trajectory due to the magnet coils (G).

Process	Upper limit	Year	Reference
$\mu^- + \mathrm{Pb} \to e^- + \mathrm{Pb}$	$< 4.6 \times 10^{-11}$	1996	[19]
$\mu^- + \mathrm{Ti} \to e^- + \mathrm{Ti}$	$< 6.1 \times 10^{-13}$	1999	[20]
$\mu^- + \mathrm{Au} \to e^- + \mathrm{Au}$	$< 7 \times 10^{-13}$	2006	[18]

Table 2: Upper limits on muon conversion branching fractions as found in the SINDRUM II experiment at PSI.

The vast majority of μ-DIO electrons does not reach the tracking detectors due to the magnetic field, while an acceptance in the region of interest of about 50% can still be maintained.

An incoming beam particle of typical momentum returns periodically to the spectrometer axis about every 65 cm, which is why the gold target is shaped as a 65 cm long tube. It is preferable to select a higher-Z material target such as gold, since the higher muon binding energy results in a lower μ-DIO fraction. Furthermore the kinematical μ-DIO endpoint rises for lower-Z material and therefore the target is of high purity to avoid low- and medium-Z material contaminations.

The muon beamline is the same one that is currently used for MEG and will be used for the MEG II and Mu3e experiments. To obtain a pulsed muon beam needed to minimize the prompt beam-related background, proton bursts of 0.3 ns hit the pion production target every 19.75 ns. The number of pions reaching the stopping target is suppressed by a CH_2 degrader at the entrance of the beam solenoid in order to minimize the RPC inside the target. The thickness of the degrader is selected such that the probability for a muon to cross the degrader is as high as possible while keeping the crossing probability for a pion of the same momentum as low as possible. This process leads to a loss of about 30% in muon intensity. The central muon momenta are 52 MeV/c and 53 MeV/c, which is low enough for the μ-DIF background to be negligible.

The electron trajectories are measured by two concentric drift chambers (E and F). The main scintillator detector (D), which consists of a cylindrical array of 64 plastic scintillator elements with PMTs on both ends of each element, is placed just inside the inner drift chamber (E) to define the start time and the direction of motion of the electron trajectories inside the drift chambers. At both ends of the tracking region cylindrical scintillation (D) and Cherenkov (C) detectors, referred to as end-cap detectors, provide extra

timing information in order to help resolving event reconstruction ambiguities. The scintillation and Cherenkov detectors are also used for triggering information, which will not be further discussed in this thesis. The spectrometer acceptance requires the electrons to cross the inner drift chamber at least once before passing through one of the end-cap detectors. This requirement implies that electrons will be measured after following a half turn trajectory, which will minimize the impact of multiple scattering on the momentum resolution, based on the same principle that will be applied in the detector design of the Mu3e experiment. The resulting momentum resolution is essential for the suppression of the μ-DIO background.

The magnet return yoke (H) on top of the spectrometer helps to suppress the cosmic ray photon background creating an e^+-e^- pair inside the target, which is the only type of cosmic ray background that cannot be identified by an incoming particle.

2.3.2 The DeeMe experiment

In 2010 an experimental search for muon conversion at the Japan Proton Accelerator Research Complex (J-PARC) has been proposed aiming for a sensitivity of 10^{-14}, which is an improvement of nearly two orders of magnitude with respect to the current experimental upper limit [21]. DeeMe (Direct Emission of Electrons by Muon-Electron conversion [22]) should be able to provide an intermediate result earlier than the larger-scale Mu2e and COMET experiments aiming for an another two orders of magnitude smaller upper limit, due to less complex design, the shorter time scale and lower costs. This section strongly relies on references [21] and [23], unless stated otherwise.

The experimental setup can be seen in Figure 11. Muonic atoms are formed inside a silicon carbide rotation* target, from where the potential conversion electrons with momentum 105 MeV/c† and other background particles are emitted into a transport beamline. The expected muonic atom formation rate inside the rotation target is 10^{10} per second. As opposed to the previous described muon experiments, the DeeMe primary proton target is both the pion production target and the muon stopping target at the same time.

*The energy deposition inside the target due to proton collisions will be spread by rotating it to avoid too high temperatures.

†the conversion electron energy $E_{\mu e}$ is 105.1 MeV for carbon and 105.0 MeV for silicon

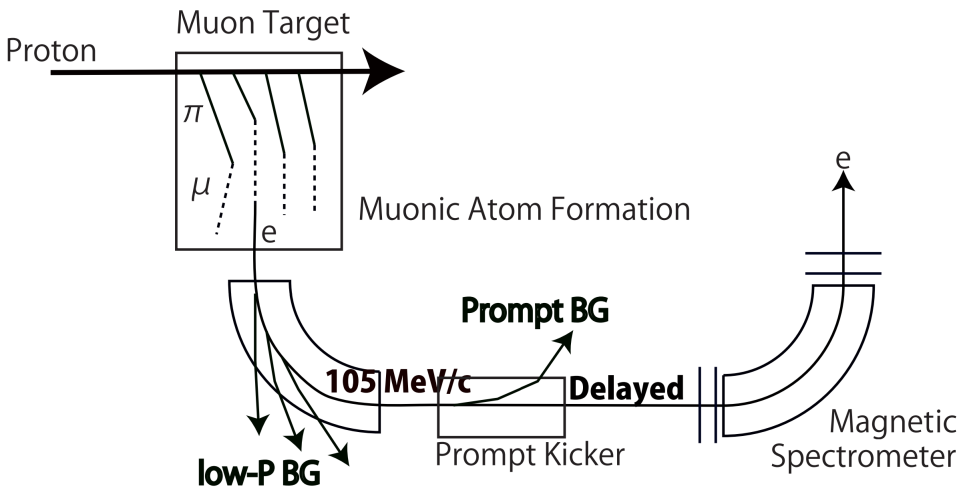

Figure 11: Schematic layout of the DeeMe experiment, adapted from [23].

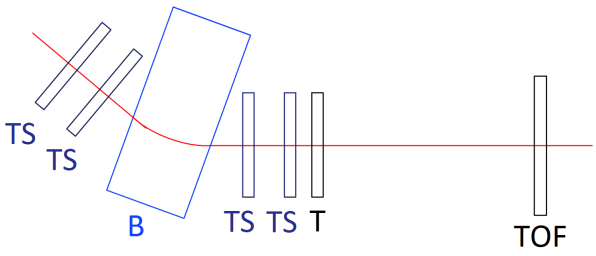

Figure 12: Schematic layout of the DeeMe magnetic spectrometer. TS: Tracking station, B: Dipole magnet, T: Trigger scintillation counter, TOF: Time-of-flight scintillation counter. Adaptation from [21]

The pulsed proton beam is extracted from the high-intensity Rapid Cycle Synchrotron (RCS) booster.

The transport beamline, called H-line (High-momentum Decay Muon port), will be constructed so that the transmission efficiency is 100%, which is important for the statistical significance of the experiment. In the magnetic field located in the first part of the H-line most of the background particles with low momentum are filtered out, which are mainly the Michel electrons and positrons. The beam successively passes kicker magnets* in order to reduce the prompt background electrons of which the rate is estimated to be 10^7 per proton pulse to a rate of 10^3-10^4 per pulse.

A schematic layout of the magnetic spectrometer is shown in Figure 12. It consists of four tracking systems, a dipole magnet, a trigger scintillation counter and a time-of-flight (TOF) scintillation counter. Each tracking system contains two planar drift chambers similar to those used in the MEG experiment, placed orthogonally with respect to each other to measure the electron position in two dimensions. The trigger and the TOF plastic scintillation counters are for defining the timing and rejecting beam muon and cosmic ray muon backgrounds respectively. The counters are placed behind the tracking systems in order to minimize multiple scattering and energy loss of the signal electrons as well as the stopping of beam muons inside the spectrometer. The momentum resolution of the spectrometer will be better than 0.3 MeV/c, which is sufficient to distinguish the signal electrons from the μ-DIO electrons.

2.3.3 The Mu2e experiment

A design for another facility to search for muon conversion has been proposed by the Mu2e Collaboration at the Fermi National Accelerator Laboratory (Fermilab) in the United States for which an estimated sensitivity of 6×10^{-17} is expected, a four orders of magnitude more stringent result than the SINDRUM II upper limit [24]. The following experimental description will be strongly based on references [7] and [24], unless indicated otherwise.

The experimental setup, shown in Figure 2 in Section 2.0.1, is composed of a Production Solenoid (PS), a Transport Solenoid (TS) and a Detector

*A kicker magnet is a fast switching dipole magnet that operates for a short amount of time to deflect and thereby filter out a segment of a particle beam. In the case of muon conversion the latter are out-of-time particles.

Solenoid (DS). A high-intensity muon beam produced by a pulsed proton beam hitting a tungsten target is lead from the PS into the TS. The proton beam is extracted from the Fermilab booster and is expected to deliver 1.2 $\times 10^{20}$ protons per year. The proton bunches have been phase-rotated* into micro-bunches of 200 ns before entering the PS, so that the ratio of out-of-time to in-time protons, also called extinction, is reduced. The resultant extinction is further reduced to 10^{-10} by the use of a kicker magnet which displaces out-of-time particles inside the proton beam into a collimator.

From the TS which contains a collimator to select only low-momentum negative muons, the muon beam is lead onto the stopping target inside the DS. The muon target, which consists of a series of thin aluminium disks, is designed thick enough to stop as many muons as possible but thin enough not to significantly alter the energy of the conversion electrons. Just like the MEG detector solenoid the superconducting high field Mu2e DS contains a strong gradient field, extending along the first half of the DS which contains the stopping target. Conversion electrons emitted from the target in the direction of the TS are deflected back to the tracking detector due to the gradient field, resulting in an almost twice as large geometrical acceptance for signal events.

The field decreases towards the end of the DS so that beam-related background is rejected by deflection, of which the unstopped muons as well as the μ-DIO electrons are focussed through the gaps inside the center of the tracker and calorimeter. This background rejection leads to another advantage of the gradient field, namely the reduction of accidental activity in the detector. Unstopped muons are also absorbed by a muon beam stop which is placed at the end of the DS to reduce detector activity originating from the beam stop.

The second part of the DS occupied by the tracker and calorimeter is covered by a nearly uniform precision magnetic field allowing for momentum analysis of conversion electrons. The DS and part of the TS are surrounded by a cosmic ray veto to shield against cosmic ray background as well as to actively detect cosmic-ray muons.

*Phase rotation is a trick used to confine either the energy spread (and thus increase the width) or the width (but increase the energy spread) of a proton bunch, where the latter is applied for Mu2e.

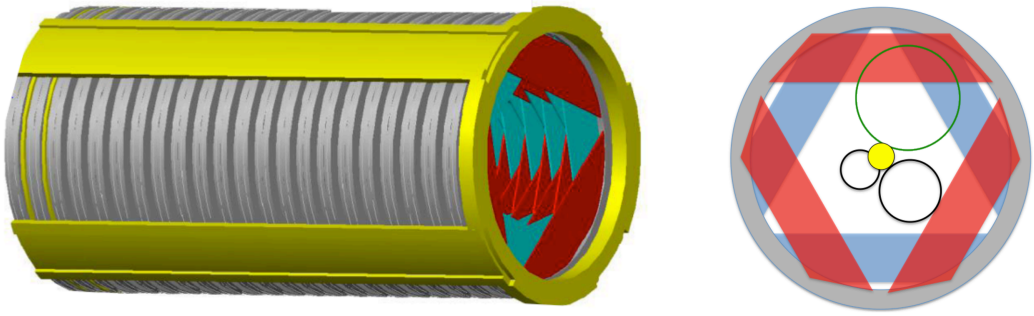

Figure 13: Schematic layout of the Mu2e straw tracker on the left and a cross sectional view of a plane on the right, including simulated tracks and the stopping target in the center*. The red and blue panels are identical double layered arrays of straws which are oriented orthogonally to the radius of the tracker. Adapted from [7].

In Figure 13 the straw tracker of about 3 m long can be seen, which has a low-mass and highly segmented design to minimize multiple scattering and to withstand high rates. The tracker is composed of ∼23,000 straw drift tubes, which are grouped in double layered arrays called panels. A tracker plane as shown on the right in Figure 13 is built out of six panels placed inside a ring. The complete tracker consists of 20 pairs of tracker planes. An advantage of straw drift tubes compared to other types of drift chambers is that failures remain isolated within a straw, thus improving the reliability. Another beneficial aspect is that because of the geometrical design all the supplementary elements such as mechanical support and readout electronics can be placed outside the radius of the active detector area.

The upper trajectory inside the cross sectional view in Figure 13 is from a simulated signal electron with a muonic aluminium conversion energy of 105 MeV. The trajectory on the lower right is from a 53 MeV Michel electron and the one on the lower left of an energy smaller than 53 MeV represents most of the μ-DIO electrons.

The calorimeter consists of two annular disks composed of 1900 scintillating crystals to provide timing and energy information. One of its main purposes is to help identify backgrounds from reconstruction errors by matching the set of measurements with those of the tracker. It can also help to reject

*Note that this is a projection of the stopping target because it is not actually inside the tracker, see Figure 2.

cosmic ray muon induced backgrounds that were not stopped by the cosmic ray veto system.

The Mu2e commissioning phase is scheduled in 2019 and data taking could then start in 2020 with an expected three year operating period. A possible upgrade of Mu2e might be realized following the proposed high-intensity upgrade to the Fermilab's proton accelerator which would provide an one order of magnitude increase in the total number of stopped muons.

2.3.4 The COMET experiment

Another future muon conversion experiment with a similar setup to Mu2e and almost the same sensitivity aim of less than 10^{-16} is COMET (COherent Muon to Electron Transition), which is currently under development at J-PARC [25]. This section relies heavily on references [25], [26] and [27], unless stated otherwise.

The experiment will be staged in two phases so that COMET Phase-I can provide useful information settling the uncertainties related to new and therefore unknown techniques for the full-sized COMET experiment (COMET Phase-II). Apart from collecting experimental data to prepare for the final phase experiment, a search for muon conversion during COMET Phase-I with an expected sensitivity of 3×10^{-15} will take place starting in 2018.

The experimental configuration of both phases is displayed in Figure 14. Both configurations consist of a proton beam line section (not pictured), a muon beam line section containing both pion capture solenoids and muon transport solenoids and a detector section.
Proton bunches extracted from the same RCS booster providing protons for the DeeMe experiment are injected into the J-PARC main ring (MR) and succeedingly hit the graphite production target inside the pion capture section. The pulse structure of 100 ns wide bunches separated by about 1 μs, very similar to Mu2e's pulse structure, helps to suppress beam-related prompt background. There are two possible schemes devised using kicker magnets in the MR to improve the proton extinction for further suppression of beam-related background events (see page 18 of ref. [25]).

The solenoid magnet surrounding the production target produces a high field that collects pions going backwards with respect to the proton beam to remove high-energy particles from the beam, while also increasing the muon intensity. Although the principle of a counterdirected proton beam to ob-

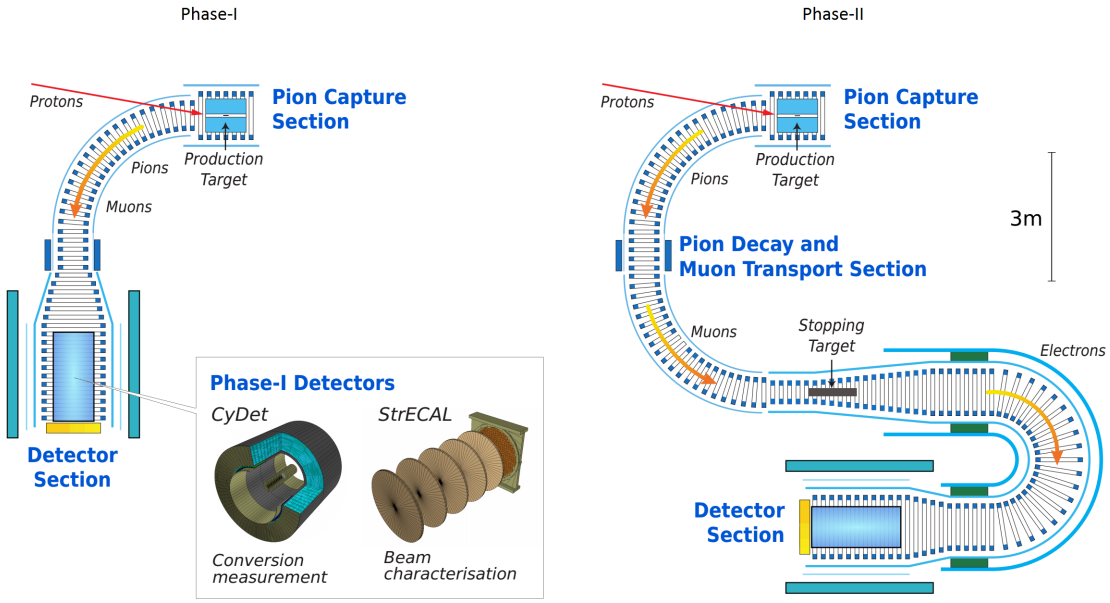

Figure 14: Schematic configuration of the two COMET phases. Adapted from [26].

tain low momentum pions is not a novel approach, the implementation of a solenoidal magnetic field to capture these pions is a main innovation. A total of $10^{18} - 10^{19}$ muons per year is expected to be produced and an estimated number of 2×10^{18} muons per year will be stopped on the muon target.

COMET Phase-I

For COMET Phase-I, aiming for a factor 100 improvement to the current upper limit, only the first curved muon transport solenoid will be constructed, which will be supplemented by a straight solenoid and another curved solenoid for Phase-II. After the 90° bend the beam passes a collimator to reduce beam-related backgrounds and is led directly into the detector section, containing either a cylindrical detector (CyDet) for conversion measurements or a straw tube tracker paired with a crystal electromagnetic calorimeter (StrECAL) for measurements of the proton beam extinction and other potential background sources.

Even though the StrECAL is the prototype detector for Phase-II, the CyDet will be used for the muon conversion search during phase-I instead. Due to

the shorter distance between the production target, stopping target and the detector in Phase-I, the StrECAL is expected to be less sensitive than the CyDet because of high occupancy in its central region from low energy beam particles and μ-DIO electrons.
The CyDet, placed inside a superconducting solenoid magnet, consists of a muon stopping target surrounded by a cylindrical drift chamber (CDC) which is complemented by two rings of Cherenkov trigger counters and scintillation counters at each end of the CDC. The muon stopping target is just like the Mu2e stopping target made of thin aluminium disks, where the same trade-off applies as for the Mu2e target thickness, and will be used for Phase-II as well. There are both passive and active cosmic ray shielding components, the passive component being a yoke inside the solenoid magnet as seen before in the SINDRUM II experiment.

The CDC reconstructs the trajectories of charged particles and provides precise momentum measurements, while the Cherenkov and scintillation counters provide trigger and timing information. The radial size of the CDC is set to create a momentum threshold of about 70 MeV/c, so that most of the prompt beam-related background and the μ-DIO events will not reach the CDC. Research on the trigger counters is ongoing and therefore the final trigger type might differ from the current rings.

As the CyDet can detect both positively and negatively charged particles as opposed to the Phase-II detector where the curved electron transport solenoid selects only negatively charged particles, a parallel search for the $\mu^- A \to e^+ A$ process will be performed. Furthermore the never before measured $\mu^- e^- \to e^- e^-$ process will be searched for, achievable because of the large geometrical acceptance of the CyDet which enables a coincidence measurement.

The StrECAL detector is regarded as a final prototype for the Phase-II detector and is used in Phase-I to profile the muon beam by identifying the beam particles and their momenta. This beam characterization should help to understand the production target distributions, transport beam optics, momentum distributions and the impurity rate.
The StrECAL is similar to the Mu2e detector configuration, consisting of a tracking system built of straw tube gas chambers accompanied by a crystal calorimeter inside a solenoid magnet. The tracking system contains five (possibly more in Phase-II) straw tube tracker stations with the possibility

of converters* inserted in between to be able to measure the direction of beam photons.

COMET Phase-II

Instead of being lead directly into the detector, the muon beam for Phase-II first passes through a C-shaped transport solenoid and is then stopped in the muon stopping target, after which the electrons pass through another curved solenoid before finally arriving at the detector. Curved solenoids enable a selection of electric charge and momentum of beam particles, a feature which is further enhanced by adding compensation magnetic dipole fields.

Just like the pion capture system, the combination of the curved solenoids, superimposed vertical dipole fields and collimators in the muon transport section is a novel approach to filter out high-momentum beam-related background while maintaining a high muon intensity.

An essential difference between the COMET and the Mu2e experiment is the shape of the muon transport solenoids, as the COMET transport section is C-shaped and the Mu2e transport section has an S-shape. The COMET transport system with a net bending angle of 180° will therefore provide a better momentum separation than the Mu2e transport section, since different circular paths of various radii originating from the same point will be furthest apart from each other after half a turn.

Another clear distinction between the two experiments are the curved electron transport solenoids following the stopping target in the COMET detector section, whereas the Mu2e stopping target is directly followed by the tracker. The curved electron transport section combined with a tuned dipole field provides the same momentum selection principle as the muon transport section, reducing backgrounds by removing particles of low momenta (less than 80 MeV/c) which are mostly μ-DIO electrons. Additionally, neutral particle hit rates will be suppressed as well because there is no line of sight between the stopping target and the detector. Therefore the probability of false-tracking due to high counting rates is reduced significantly, with detection hit rates of about 1000 hits per second, whereas the Mu2e experiment expects already for a single straw tube a 500 times higher hit rate.

The muon stopping target is placed inside a gradient magnetic field in Phase-

*converts a photon into an electrical signal via pair production or the photo-electric effect

II to capture backward emitted electrons, just like in the Mu2e detector section. It is followed by a beam blocker to suppress beam-related backgrounds. The last part of the detector section is the StrECAL detector from Phase-I, or a very similar one. The detector, which is placed inside a uniform solenoidal magnetic field, distinguishes electrons from other particles and measures their momenta with the straw tube tracker and their energies with the electromagnetic calorimeter. The calorimeter also provides timing information and trigger signals, as well as additional position measurements to suppress reconstruction errors.

PRISM

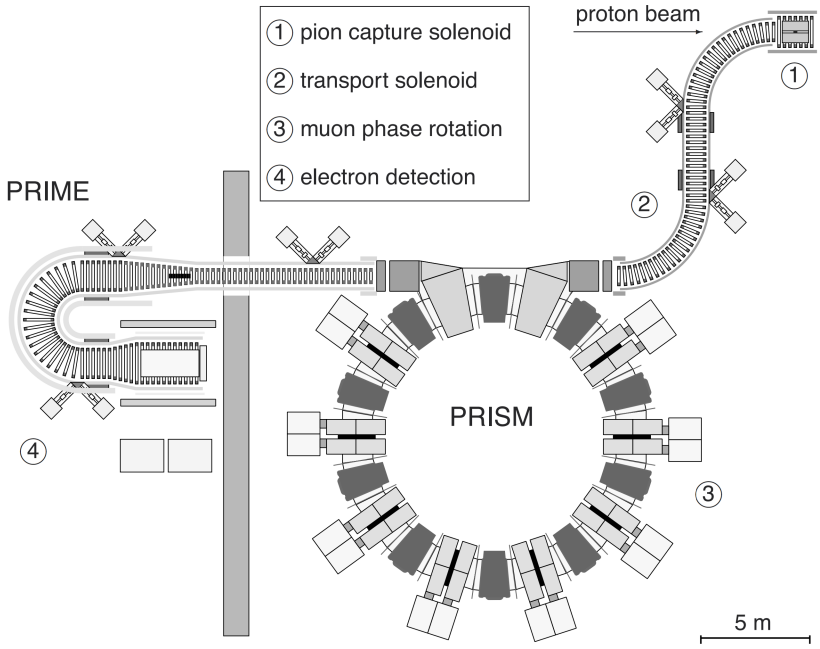

Figure 15: Schematic layout of the PRISM/PRIME experiment. The PRIME (PRIsm Mu-E conversion) detector for the PRISM experiment is conceptually similar to the COMET detector [28]. Taken from ref. [27].

A long-term upgrade for the COMET experiment aiming for a sensitivity of order 10^{-18} and beyond is the PRISM (Phase Rotated Intense Slow Muon source) project, which will include the PRISM muon storage ring as can be

seen in Figure 15 [28]. This prospective experiment has to make use of a future proton accelerator of higher beam power than currently available to increase the number of stopped muons. Another important statistical factor is the use of a stopping target made of high-Z material such as gold, which is possible if the beam pion contamination is kept below a level of 10^{-20} in order to have a negligible prompt background level. This can be achieved with the PRISM ring where muons can be kept inside for many turns until the pions have decayed out. Also essential when adopting a heavy stopping target is to suppress the out-of-time particles to a negligible level because of the relatively short muonic atomic lifetimes. Fast kicker magnets will therefore be installed at the injection and extraction part of the muon storage ring to enhance the muon beam extinction.

An additional requirement for the stopping target is a small thickness to obtain high momentum resolution, which has to be compensated by a narrow energy spread of the muon beam, since the muons with the highest energy should determine the target thickness for an optimal muon stopping efficiency. Therefore the muons will be phase-rotated inside the storage ring to acquire a narrow energy spread, which is the same method used in the Mu2e experiment but with an opposite effect.

2.4 Concluding remarks

Promising projects are on the way for each of the three channels. Current upper limits of the order of $10^{-12} - 10^{-13}$ by the MEG, SINDRUM and SINDRUM II experiments will be significantly improved, with expected sensitivities almost reaching down to the 10^{-17} level for the muon conversion experiments (Mu2e, COMET). The future muon conversion projects are able to reach the smallest upper limits because of the high conversion rates and the mono-energetic signal event which is far above the endpoint of the Michel decay spectrum and which allows for high rates without accidental background. For $\mu \to e\gamma$ and $\mu \to eee$, the expected sensitivities are at the level of 10^{-14} (MEG II) and 10^{-16} (Mu3e), respectively.

3 Other decays

In this chapter, the searches for several other lepton flavor violating decays and processes will be described besides those using muons.

3.1 Tauon decays

This section relies strongly on references [2], [8] and [29], unless stated otherwise.

Another channel of cLFV experiments are the tauon decays, which are conceptually quite similar to searches for muon decays. Just as the $\mu \to e\gamma$ decay, a possible tauonic cLFV decay is $\tau \to \ell\gamma$, where ℓ is either a muon or an electron. The dominant background of the standard model $\tau \to \ell\nu\bar{\nu}$ decay coinciding with a photon from another decay is for example analogous to the accidental background for $\mu \to e\gamma$ as discussed in Section 2.1. The equivalent for $\mu \to eee$ is $\tau \to \ell\ell\ell$, but tauon conversion does not exist due to the extremely short tauon lifetime of only 2.91×10^{-13} s [4].
As discussed in Chapter 2 also here detector energy, momentum and timing resolutions for particle identification, tracking reconstruction and calorimetric measurements are of prime importance.

Since the tauon weights about 17 times the muon mass, it has many more decay modes than the muon since besides leptons hadrons are also possible decay products. Therefore a wide variety of tauonic cLFV modes are being and have been studied, as depicted on the horizontal axis in Figure 16 [4]. Their correspondent upper limits reaching down to 10^{-8} are significantly larger than recent upper limits on muon branching fractions and the reasons for this will be discussed below.

Another consequence of the short tauon lifetime is that a tauon beam cannot be realized. Hence yielding a high tauon intensity to search for events of small occurrence is more difficult than for muon experiments, leading to lower sensitivities. Instead tauons are, for example, produced in tau-antitau pairs at e^+e^- colliders such as BaBar (United States) and Belle (Japan) by the $e^+e^- \to \tau^+\tau^-$ process. In fact these e^+e^- colliders are B meson factories optimized for the $e^+e^- \to B\bar{B}$ process, but they serve as τ factories as well since almost as many $\tau^+\tau^-$ pairs as $B\bar{B}$ pairs are produced. The LHCb experiment at CERN provides τ's from proton collisions.

Secondly, the many possible decay modes of the tauon lead to a relatively

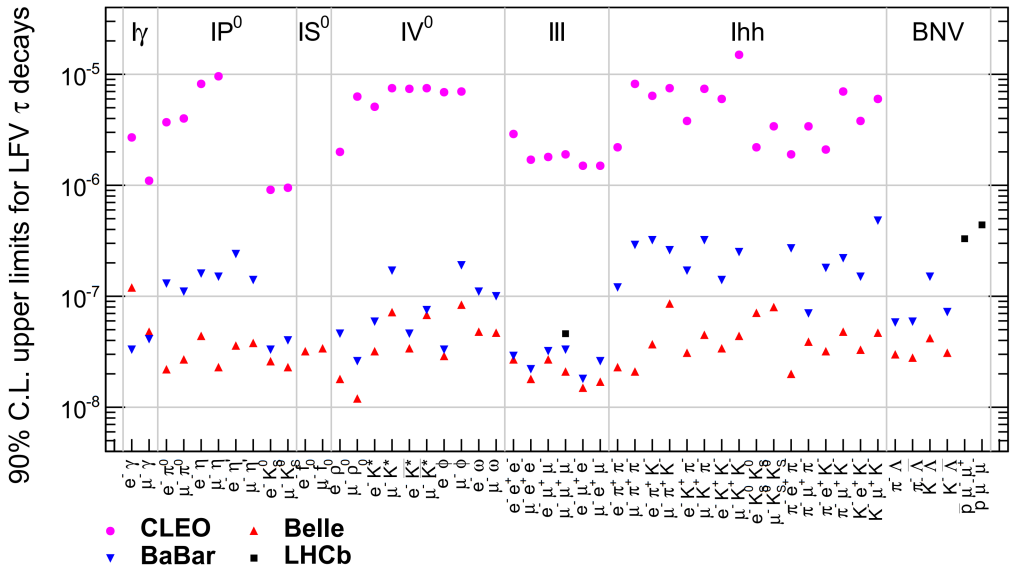

Figure 16: 90% C.L. upper limits of cLFV tauon decay branching ratios as summarized in summer 2014 by HFAG. Adapted from ref. [30].

smaller branching fraction for each tauonic LFV mode, which also reduces the respective sensitivity. Finally, the absence of a tauon conversion process might also be seen as a reason why tauon decay searches will provide larger, thus less stringent, upper limits than searches for muon decays, since the prospects for the sensitivities of Mu2e and COMET are significantly higher than for MEG II and Mu3e.

Future perspectives in Japan [31], Italy [32] and at LHCb [33] are expected to increase sensitivities to an order of 10^{-9} to 10^{-10}.

3.2 Meson decays

Many parts of this section rely greatly on reference [34], other references will be cited accordingly.

As opposed to cLFV muon decays where the lepton number L equals 1 for both the initial and final state, the initial state of a cLFV meson decay has lepton number L=0. Whereas the previously discussed muon cLFV processes are only lepton flavor violating, meson decays can therefore also be lepton number violating, which is inherently lepton flavor violating as well. The reverse does not necessarily hold, a meson decay into $e^+\mu^-$ for example is not lepton number violating, but it does violate lepton flavor.

Meson cLFV searches are often performed and their results published as an addition to other related non-LFV modes, in contrast to muon cLFV searches. We can look in literature for existing limits, of which an indicative selection is summarized in Table 3, ordered by their sensitivities. Except for a few pion and kaon limits, most of the present upper limits are of comparable

Process	Upper limit (90% C.L.)	Experiment	Year	Ref.
$D_S^+ \to K^+ e^- \mu^+$	9.7×10^{-6}	BaBar	2011	[35]
$\Upsilon(3S)^{\parallel} \to \mu^\pm \tau^\mp$	3.1×10^{-6}	BaBar	2010	[36]
$\phi \to e^\pm \mu^\mp$	2×10^{-6}	SND†	2010	[37]
$D^+ \to K^+ e^+ \mu^-$	1.2×10^{-6}	BaBar	2011	[35]
$D^0 \to e^\pm \mu^\mp$	2.6×10^{-7}	Belle	2010	[38]
$J/\psi \to e^\pm \mu^\mp$	1.6×10^{-7}	BESIII‡	2013	[39]
$B^{\P} \to K e^\pm \mu^\mp$	3.8×10^{-8}	BaBar	2006	[40]
$B_S^0 \to e^\pm \mu^\mp$	1.1×10^{-8}	LHCb	2013	[41]
$B^0 \to e^\pm \mu^\mp$	2.8×10^{-9}	LHCb	2013	[41]
$\pi^0 \to \mu^+ e^- + \mu^- e^+$	3.6×10^{-10}	KTeV§	2008	[42]
$K^+ \to \pi^+ \mu^+ e^-$	1.3×10^{-11}	BNL E865	2005	[43]
$K_L^0 \to e^\pm \mu^\mp$	4.7×10^{-12}	BNL E871	1998	[44]

Table 3: Selection of some of the most stringent limits on the branching ratios of meson cLFV processes [4].

$^{\parallel}$the third resonance or excited state of the Υ meson
†the SND detector at the VEPP-2M collider in Russia
‡the BESIII detector at the BEPCII collider in China
$^{\P}B^+$ or B^0
§the KTeV experiment at Fermilab in the United States

order of magnitude as the tauon limits (Section 3.1) and hence also far above the sensitivities reached in muon experiments.

We will mainly focus on B and D meson decays and given statements will thus apply to these mesons, but they don't neccessarily have to hold for all mesons. Experimental methods will be illustrated by a brief discussion of the two B factories Belle and BaBar where B mesons are produced through e^+e^- collisions, as well as the LHCb experiment creating mesons through proton collisions, each operating at an energy scale favorable for $B\bar{B}$ production. As we will go through these different analyses, several reasons for meson limits being less stringent than the muon limits will be made clear.

As for tauon decays, mesons are also heavy particles and thus have many different decay modes. Most decays can typically be sorted into one of the two following decay modes: a 2-body $M \to \ell\ell'$ meson decay into two leptons or a 3-body $M \to M'\ell\ell'$ meson decay into another meson together with two leptons.

Normal leptonic decay modes consist of a lepton and an antilepton of the same (anti-)flavor. An example of this is the following decay of the strange B meson: $B_S^0 \to e^+\nu_e\,\mu^-\bar{\nu}_\mu$. Without the neutrinos, this would be a cLFV process. It is therefore of prime importance that the initial state energy and momentum are clearly defined in a cLFV experiment so that one can be sure whether the neutrinos, which are undetectable, have carried away any energy and momentum.

Both tauons and heavy mesons cannot be detected directly due to their short lifetimes and thus they can only be detected through their decay products. Decay modes containing a tau lepton tend to be more difficult to access experimentally because of the multiple decay modes of the tauon and missing energy caused by neutrinos. A subsequent $\tau \to \ell\nu\bar{\nu}$ decay would for example provide no kinematical constraints to be exploited experimentally. This is also why most of the decay modes listed in Table 3 feature only electrons and muons. Consequently searches for meson decays involving tauons require special experimental techniques such as hadronic tag reconstruction (see Section 7.4.1 of ref. [34]) for hadronic tau decays, which leads to lower sensitivities due to limited signal efficiencies.

A major difference between meson (and also tauon) and muon experiments is the required level of particle identification (PID). Since the lifetimes of heavy mesons are very short (of the same order as the tauon lifetime [4]), they cannot be measured directly and therefore they have to be identified

indirectly by their decay products. Detectable decay products are charged particles which are relatively stable, namely electrons, muons, pions, kaons and protons. PID is essential in background suppression by separating different types of hadronic decay modes such as $\pi^+\pi^-$, $K^\pm\pi^\mp$ and K^+K^- as well as by the flavor-tagging* of B mesons.

Just as in muon experiments, background rejection is also implemented by setting momentum constraints and topological constraints.

The scope of PID also requires the detectors to be much more complex than the detector systems for muon experiments, since they have to be sensitive to a much greater range of decay modes, types of particles and particle momenta. Another complicating factor are the high momenta produced in the e^+e^- collisions (or pp collisions in the case of LHCb), leading to more complicated particle detection compared to the low momenta in muon experiments. This is hence an important limiting factor on the sensitivity.

Muon conversion, the most precise muon mode because of the mono-energetic signal and high conversion rates, does not exist for mesons due to their short lifetime, which is just as for the tauon experiments one of the reasons why meson experiments cannot reach similar sensitivities as muon experiments.
The schematic detector layouts of Belle, BaBar and LCHb are displayed in Figure 17, 18 and 19 respectively. Belle and BaBar are conceptually quite similar, with a few differences due to the different accelerator complexes, technical competences and available resources of the collaborations.

The most evident differences between Belle/BaBar and LHCb is that the former are e^+e^- colliders, whereas LHCb is a proton collider operating at much higher energies, namely 3.5 TeV per beam in 2009 which has meanwhile developed to 7 TeV per beam [41,48]. An indication for Belle/BaBar energies is depicted in Figure 17. As a consequence LHCb can produce many more B mesons but also suffers from large backgrounds, whereas Belle and BaBar can retrieve a more clean signal.
Another evident difference is the cylindrical detector shape of Belle/BaBar where the collision takes place in the middle of the detector versus the planar shape of LHCb where the proton beams collide inside the vertex locator.

Regarding the individual components of the detector, the detectors contain a lot of elements that are familiar from the detectors in Chapter 2: superconducting solenoids, the LHCb dipole magnet (DeeMe, Section 2.3.2),

*determining whether it contains a b quark or a $\bar{b}$ quark

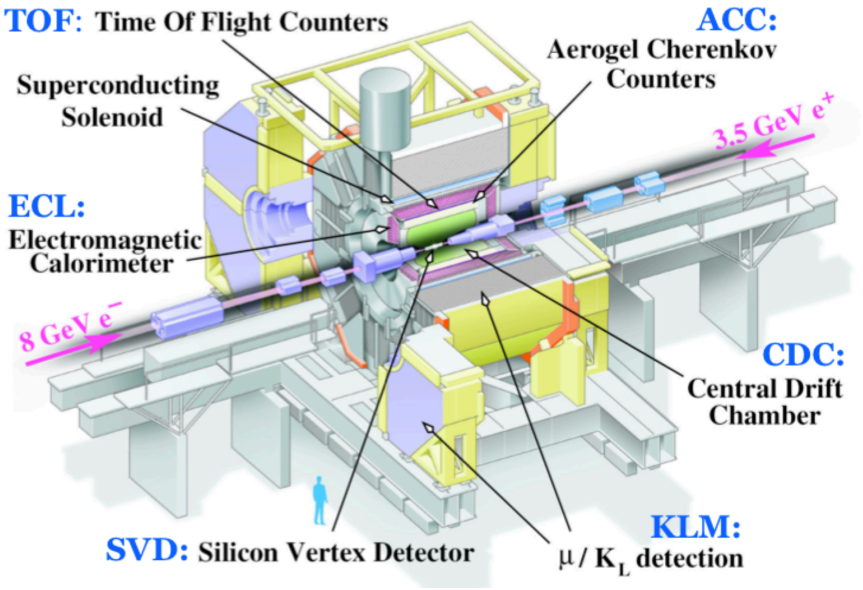

Figure 17: The Belle detector. From [45].

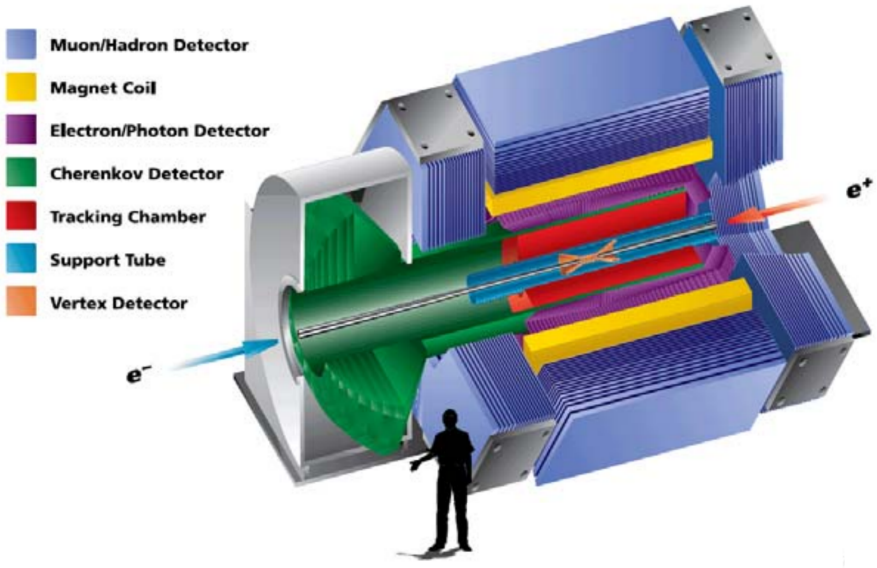

Figure 18: The BaBar detector. From [46].

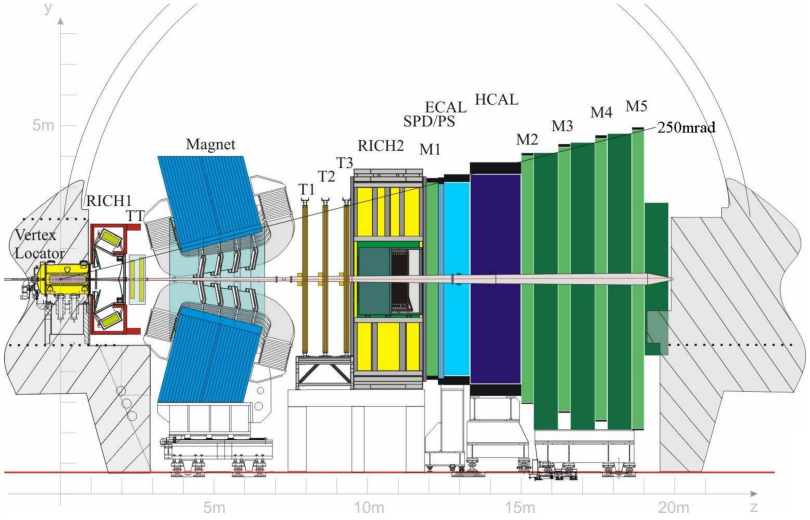

Figure 19: The LHCb detector. RICH: Ring Imaging Cherenkov detector, TT: Trigger Tracker, T: Tracking station, M: Muon system, SPD: Scintillating Pad Detector, PS: PreShower, ECAL/HCAL: electromagnetic/hadronic calorimeter [47]. From [48].

time-of-flight counters (DeeMe), Cherenkov counters (SINDRUMII, Section 2.3.1 and COMET, Section 2.3.4), drift chambers (all experiments in Chapter 2 except for Mu3e, Section 2.2.2), silicon vertex detectors (Mu3e), an electromagnetic calorimeter (Mu2e, Section 2.3.3 and COMET) and scintillator detectors (all except for Mu2e). Even though most individual components are similar to those used in the detectors for muon decays, the meson experiments are composed of many more elements, including components which are not needed for muon experiments such as LHCb's PreShower, muon/hadron detectors and hadronic calorimeters.

Future prospects are the Belle II upgrade for the Belle experiment in Japan [31], the SuperB project in Italy [32], an upgraded accelerator complex at Fermilab giving opportunities for rare kaon decay searches [49] and further searches at the LHCb [33].

3.3 Miscellaneous decays

3.3.1 Z^0 and Higgs boson decay

A recent search for $Z \to e\mu$ has been conducted with the ATLAS detector, which is just like LHCb one of the detectors at the Large Hadron Collider (LHC) at CERN [50]. The resulting upper limit on the branching fraction of 7.5 $\times 10^{-7}$ (95% C.L.) has been published in 2014. There has been only one other experiment looking for Z^0 cLFV modes in 1996, which was the DELPHI experiment that was once located at CERN as well [4, 51].

Future searches for cLFV Z^0 decays can be expected from the LCHb and the other particle detectors at CERN, as well as from Belle II and other prospective meson factories as spin-off results from searches for Z^0 decay modes of higher priority. The same statement holds for Higgs decay, as CERN plans to conduct precision measurements on the Higgs boson with ATLAS and CMS and also to increase the luminosity of the LHC by a factor 10, which should increase the feasibility to search for a cLFV mode as a by-product as well [52, 53].

3.3.2 Neutrinoless double beta decay

Another cLFV channel which has been extensively researched is the $A \to A^* + 2e^-$ decay, commonly known as neutrinoless double beta decay. This process is obviously lepton flavor violating because of lepton number violation by $\Delta L = 2$. For a review and results on this topic, see ref. [54].

3.3.3 Muonium to antimunonium conversion

The spontaneous muonium to antimuonium conversion ($\mu^+e^- \to \mu^-e^+$) where $\Delta L = 0$ but $\Delta L_e = -\Delta L_\mu = 2$ has been searched for at PSI in 1998, following a number of earlier attempts [55]. An upper limit on the branching ratio of 8.2 $\times 10^{-11}$ (90% C.L.) has been established. Future experiments might be planned at facilities with high-intensity pulsed muon beams [56].

4 Discussion and conclusions

Until now no cLFV process has been seen and as a result the experimental outcomes are expressed in upper limits on the branching ratio. However, promising future projects such as MEG II (Section 2.1.2), Mu3e (Section 2.2.2), Mu2e and COMET (Section 2.3.3 and 2.3.4) might produce a positive result or otherwise significantly improve the upper limits.

The muon experiments provide the most stringent results, since muons are more stable than tauons and mesons, allowing them to form high-intensity muon beams which greatly enhances the statistics of an experiment. Furthermore, the muon has much less possible decay modes than tauons and mesons because of its smaller mass, enabling the detectors to be more specified for certain particles and corresponding energies, which enhances the precision of the experiment.

A crucial requirement for a successful measurement is a background suppession below the level of the aimed sensitivity. Hence minimizing the background while also maintaining high muon intensities sets a serious challenge for these experiments. Other essential detector conditions are excellent momentum, energy, vertex and timing resolutions, high geometrical acceptance and high detector efficiencies. A lot of muon detectors are built in a cylindrical shape, enclosing the stopping target in the middle. This design is often used because the unstopped beam particles can leave the experiment without hitting the detector, resulting in lower background activity and less detector hit rates. Another advantage of the cylindrical detector is that the radial size can easily be adjusted to provide an easy method for momentum selection.

It has further been shown that tauon and meson decay searches have many similarities, from the many possible decay modes to the production and measurement facilities.

Other cLFV processes such as Z^0 boson decay, neutrinoless double beta decay and muonium to antimuonium conversion have been studied experimentally as well and corresponding upper limits have been set.

5 Acknowledgements

I would like to thank Prof. Y. Kuno from the Osaka University and Prof. A. van der Schaaf from the University of Zurich for providing the answers for some questions I've had about the SINDRUM II experiment and the DeeMe experiment.

I would also like to thank Rosa Kappert for being involved with my research and for being available to answer any questions related to my research.

Most importantly I would like to thank my supervisor Gerco Onderwater for his continuous enthusiasm, the inspiring discussions and his dedication. I could not have wished for a better supervisor and I am extremely thankful for the continuous time and effort he has put into guiding me through my thesis, even though the process has taken much longer than what is common.

References

[1] Chris Vos. Overview of the theoretical status of cLFV, *http://irs.ub.rug.nl/dbi/55a36eb6daf4d* (retrieved at 24/02/2016), 2015.

[2] F. Cei and D. Nicolò. Lepton Flavour Violation Experiments. *Advances in High Energy Physics*, Mar 2014.

[3] Wolfgang Pauli. Letter from Pauli to a group of nuclear physicists in *Tübingen*, *http://www.symmetrymagazine.org/article/march-2007/neutrino-invention* (retrieved at 22/03/2016), Dec 1930.

[4] K.A. Olive. Review of Particle Physics. *Chinese Physics C*, 38(9):090001, Aug 2014.

[5] E. P. Hincks and B. Pontecorvo. Search for Gamma-Radiation in the 2.2-Microsecond Meson Decay Process. *Phys. Rev.*, 73:257 –, Feb 1948.

[6] A. M. Baldini, F. Cei, C. Cerri, et al. MEG Upgrade Proposal. *arXiv:1301.7225v2*, Feb 2013.

[7] L. Bartoszek, E. Barnes, J. P. Miller, et al. Mu2e Technical Design Report. *arXiv:1501.05241*, Jan 2015.

[8] Y. Kuno. Rare lepton decays. *Progress in Particle and Nuclear Physics*, May 2015.

[9] E. Ripiccini. New result from the MEG Experiment at PSI and the MEG upgrade. *Nuclear and Particle Physics Proceedings*, Mar 2015.

[10] J. Adam, X. Bai, A. M. Baldini, et al. The MEG detector for $\mu^+ \to e^+\gamma$ decay search. *Eur. Phys. J. C*, 73(4), Apr 2013.

[11] J. Adam, X. Bai, A. M. Baldini, et al. New Constraint on the Existence of the $\mu^+ \to e^+\gamma$ Decay. *Phys. Rev. Lett.*, 110(201801), May 2013.

[12] Niklaus Berger. The Mu3e Experiment. *Nuclear Physics B - Proceedings Supplements*, Mar 2014.

[13] W. Bertl, S. Egli, R. Eichler, et al. Search for the decay $\mu^+ \to e^+e^+e^-$. *Nuclear Physics B*, Oct 1985.

[14] U. Bellgardt, G. Otter, R. Eichler, et al. Search for the decay $\mu^+ \to e^+e^+e^-$. *Nuclear Physics B*, Mar 1988.

[15] A. Blondel, A. Bravar, M. Pohl, et al. Research Proposal for an Experiment to Search for the Decay $\mu \to eee$. *arXiv:1301.6113v1*, Jan 2013.

[16] Y.G. Cui, R. Palmer, Y. Arimoto, et al. Conceptual Design Report for Experimental Search for Lepton Flavor Violating $\mu^- - e^-$ Conversion at Sensitivity of 10^{-16} with a Slow-Extracted Bunched Proton Beam (COMET). Jun 2009.

[17] R. J. Abrams, D. Alezander, G. Ambrosio, et al. Mu2e Conceptual Design Report. *arXiv*, Nov 2012.

[18] W. Bertl, R. Engfer, E.A. Hermes, et al. A search for μ-e conversion in muonic gold. *The European Physical Journal C*, May 2006.

[19] W. Honecker, C. Dohmen, H. Haan, et al. Improved Limit on the Branching Ratio of $\mu \to$ e Conversion on Lead. *Physical Review Letters*, Jan 1996.

[20] H. V. Klapdor-Kleingrothaus and I. V. Krivosheina, editors. *Lepton and baryon number violation in particle physics, astrophysics and cosmology. Proceedings, 1st International Symposium, Lepton-baryon'98, Trento, Italy, April 20-25, 1998*. 1999.

[21] M. Kinsho, M. Ikegami, N. Kawamura, et al. Proposal of an Experimental Search for μ-e Conversion in Nuclear Field at Sensitivity of 10^{-14} with Pulsed Proton Beam from RCS. Dec 2010.

[22] S. Mihara. Muon physics programs at J-PARC. *Presented at Physics of fundamental Symmetries and Interactions - PSI2010*, Aug 2010.

[23] M. Aoki and DeeMe Collaboration. An experimental search for muon-electron conversion in nuclear field at sensitivity of 10^{-14} with a pulsed proton beam. 2012.

[24] David Brown. Mu2e: a Muon to Electron Conversion Experiment at Fermilab. *Nuclear Physics B - Proceedings Supplements*, Mar 2014.

[25] Y. Kuno. A search for muon-to-electron conversion at J-PARC: the COMET experiment. *Progress of Theoretical and Experimental Physics*, 2013(2):22C010, Feb 2013.

[26] Benjamin Edward Krikler. An Overview of the COMET Experiment and its Recent Progress. Dec 2015.

[27] Yoshitaka Kuno. COMET and PRISM Search for Charged Lepton Flavor Violation with Muons. *Nuclear Physics B - Proceedings Supplements*, Apr−Jun 2012.

[28] R.J. Barlow. The PRISM/PRIME Project. *Nuclear Physics B - Proceedings Supplements*, 218(1):4449, Sep 2011.

[29] S. Mihara, J.P. Miller, P. Paradisi, et al. Charged Lepton Flavor-Violation Experiments. *Annual Review of Nuclear and Particle Science*, 63(1):531552, Oct 2013.

[30] Heavy Flavor Averaging Group: Y. Amhis, Sw. Banerjee, E. Ben-Haim, et al. Averages of b-hadron, c-hadron, and τ-lepton properties as of summer 2014. Dec 2014.

[31] Boqun Wang. The Belle II Experiment and SuperKEKB Upgrade. Nov 2015.

[32] SuperB Collaboration. SuperB: A High-Luminosity Asymmetric e^+e^- Super Flavor Factory. Conceptual Design Report. Sep 2007.

[33] R. Aaij, C. Abellán Beteta, and B. Adeva. Letter of Intent for the LHCb Upgrade. Mar 2011.

[34] Ed. A.J. Bevan, B. Golob, Th. Manne, et al. The Physics of the B Factories. *Eur. Phys. J. C*, 74:3026, Jun 2014.

[35] J. P. Lees, V. Poireau, V. Tisserand, et al. Searches for rare or forbidden semileptonic charm decays. *Phys. Rev. D*, 84(7), Oct 2011.

[36] J. P. Lees, V. Poireau, E. Prencipe, et al. Search for Charged Lepton Flavor Violation in Narrow Υ Decays. *Physical Review Letters*, 104(15), Apr 2010.

[37] M. N. Achasov, K. I. Beloborodov, A. V. Bergyugin, et al. Search for lepton flavor violation process $e^+e^- \to e\mu$ in the energy region $\sqrt{s} = 984 - 1060MeV$ and $\phi \to e\mu$ decay. *Phys. Rev. D*, 81(5), Mar 2010.

[38] M. Petrič, M. Starič, I. Adachi, et al. Search for leptonic decays of D^0 mesons. *Phys. Rev. D*, 81(9), May 2010.

[39] M. Ablikim, M. N. Achasov, O. Albayrak, et al. Search for the lepton flavor violation process $J/\psi \to e\mu$ at BESIII. *Phys. Rev. D*, 87(11), Jun 2013.

[40] B. Aubert, R. Barate, M. Bona, et al. Measurements of branching fractions, rate asymmetries, and angular distributions in the rare decays $B \to K\ell^+\ell^-$ and $B \to K^*\ell^+\ell^-$. *Phys. Rev. D*, 73(9), May 2006.

[41] R. Aaij, B. Adeva, M. Adinolfi, et al. Search for the Lepton-Flavor-Violating Decays $B_S^0 \to e^\pm\mu^\mp$ and $B^0 \to e^\pm\mu^\mp$. *Physical Review Letters*, 111(14), Sep 2013.

[42] E. Abouzaid, M. Arenton, A. R. Barker, et al. Search for Lepton-Flavor-Violating Decays of the Neutral Kaon. *Physical Review Letters*, 100(13), Apr 2008.

[43] Aleksey Sher, R. Appel, G. S. Atoyan, et al. Improved upper limit on the decay $K^+ \to \pi^+\mu^+e^-$. *Phys. Rev. D*, 72(1), Jul 2005.

[44] D. Ambrose, C. Arroyo, M. Bachman, et al. New Limit on Muon and Electron Lepton Number Violation from $K_L^0 \to \mu^\pm e^\mp$ Decay. *Physical Review Letters*, 81(26):57345737, Dec 1998.

[45] O. Seon. Search for the lepton-number-violating decay B^+ to $D^-l^+l^+$ at Belle, *http://belle.kek.jp/belle/talks/PIC10/O.Seon.pdf* (retrieved at 17/03/2016), Sep 2010. XXX. Physics in Collision 2010 (PIC 2010).

[46] K. Hayasaka On behalf of Belle and BaBar. Searches for LFV at B factories, *http://belle.kek.jp/belle/talks/DISCRETE08/K.Hayasaka.pdf* (retrieved at 17/03/2016), Dec 2008. Symposium on Prospects in the Physics of Discrete Symmetries (DISCRETE 2008).

[47] R. Aaij, C. Abellan Beteta, B. Adeva, et al. Search for Lepton Number Violating Decays $B^+ \to \pi^-\mu^+\mu^+$ and $B^+ \to K^-\mu^+\mu^+$. *Physical Review Letters*, 108(10), Mar 2012.

[48] Eddy Jans. The LHCb detector. Oct 2009.

[49] Andreas S. Kronfeld, Robert S. Tschirhart, Usama Al-Binni, et al. Project X: Physics Opportunities. Jun 2013.

[50] G. Aad, B. Abbott, J. Abdallah, et al. Search for the lepton flavor violating decay $Z \to e\mu$ in pp collisions at $\sqrt{s} = 8TeV$ with the ATLAS detector. *Phys. Rev. D*, 90(7), Oct 2014.

[51] P. Abreu et al. Search for lepton flavour number violating Z^0 -decays. *Zeitschrift für Physik C Particles and Fields*, 73(2):243251, Jan 1997.

[52] Peter Vankov on behalf of the ATLAS collaboration. ATLAS Upgrade for the HL-LHC: meeting the challenges of a five-fold increase in collision rate. Jan 2011.

[53] CMS Collaboration. CMS Phase II Upgrade Scope Document. Sep 2015.

[54] K. Zuber. Neutrinoless double beta decay. Jan 2012.

[55] L. Willmann, P. V. Schmidt, H. P. Wirtz, et al. New Bounds from a Search for Muonium to Antimuonium Conversion. *Physical Review Letters*, 82(1):4952, Jan 1999.

[56] Klaus P. Jungmann. Past, Present and Future of Muonium. Apr 2004.